10-2014

Interactions of energetic electrons with ULF waves triggered by interplanetary shock: Van Allen Probes observations in the magnetotail

Y. X. Hao
Peking University

Q. G. Zong
Peking University

Y. F. Wang
Peking University

X. Z. Zhou
Peking University

Hui Zhang
University of Alaska Fairbanks

See next page for additional authors

Recommended Citation
Hao, Y. X., et al. (2014), Interactionsof energetic electrons with ULFwaves triggered by interplanetaryshock: Van Allen Probes observa-tions in the magnetotail, J. Geophys.Res. Space Physics, 119, 8262–8273,doi:10.1002/2014JA020023.

AGU PUBLICATIONS

JGR

Journal of Geophysical Research: Space Physics

RESEARCH ARTICLE

10.1002/2014JA020023

Key Points:
- IP shock drove nightside Pc 4–5 ULF wave at L = 5–6 area
- ULF wave modulated electrons with clear drift resonance at 150–230 keV
- Both wave phase comparing and resonant energy indicate an m of ~14

Correspondence to:
Q.-G. Zong,
qgzong@pku.edu.cn

Citation:
Hao, Y. X., et al. (2014), Interactions of energetic electrons with ULF waves triggered by interplanetary shock: Van Allen Probes observations in the magnetotail, *J. Geophys. Res. Space Physics*, *119*, 8262–8273, doi:10.1002/2014JA020023.

Received 1 APR 2014
Accepted 11 SEP 2014
Accepted article online 18 SEP 2014
Published online 21 OCT 2014

Interactions of energetic electrons with ULF waves triggered by interplanetary shock: Van Allen Probes observations in the magnetotail

Y. X. Hao[1], Q.-G. Zong[1], Y. F. Wang[1], X.-Z. Zhou[1], Hui Zhang[2], S. Y. Fu[1], Z. Y. Pu[1], H. E. Spence[3], J. B. Blake[4], J. Bonnell[5], J. R. Wygant[6], and C. A. Kletzing[7]

[1]Institute of Space Physics and Applied Technology, Peking University, Beijing, China, [2]Geophysical Institute, University Alaska Fairbanks, Fairbanks, Alaska, USA, [3]Department of Physics Institute for Earth, Oceans and Space, University of New Hampshire, Durham, New Hampshire, USA, [4]The Aerospace Corporation, Los Angeles, California, USA, [5]Space Science Laboratory, University of California, Berkeley, California, USA, [6]School of Physics and Astronomy, University of Minnesota, Twin Cities, Minneapolis, Minnesota, USA, [7]Department of Physics and Astronomy, University of Iowa, Iowa City, Iowa, USA

Abstract We present in situ observations of a shock-induced substorm-like event on 13 April 2013 observed by the newly launched Van Allen twin probes. Substorm-like electron injections with energy of 30–500 keV were observed in the region from L ~5.2 to 5.5 immediately after the shock arrival (followed by energetic electron drift echoes). Meanwhile, the electron flux was clearly and strongly varying on the ULF wave time scale. It is found that both toroidal and poloidal mode ULF waves with a period of 150 s emerged following the magnetotail magnetic field reconfiguration after the interplanetary (IP) shock passage. The poloidal mode is more intense than the toroidal mode. The 90° phase shift between the poloidal mode B_r and E_a suggests the standing poloidal waves in the Northern Hemisphere. Furthermore, the energetic electron flux modulations indicate that the azimuthal wave number is ~14. Direct evidence of drift resonance between the injected electrons and the excited poloidal ULF wave has been obtained. The resonant energy is estimated to be between 150 keV and 230 keV. Two possible scenaria on ULF wave triggering are discussed: vortex-like flow structure-driven field line resonance and ULF wave growth through drift resonance. It is found that the IP shock may trigger intense ULF wave and energetic electron behavior at L ~3 to 6 on the nightside, while the time profile of the wave is different from dayside cases.

1. Introduction

Interplanetary shocks (IP shocks) associated with solar ejecta have been known as one of the most intense external drivers of the magnetospheric dynamics [e.g., *Gosling et al.*, 1991; *Gosling*, 1993; *Keika et al.*, 2008; *Zong et al.*, 2009; *Yue et al.*, 2010, 2011]. The interaction between IP shocks and the magnetosphere is usually dominated by the compression of the entire magnetosphere [e.g., *Nishida and Maezawa*, 1971; *Huttunen et al.*, 2005; *Keika et al.*, 2008; *Zong et al.*, 2009] when IP shocks impinge on the Earth's magnetosphere. Statistical studies [*Yue et al.*, 2009, 2010, 2011] have shown that after the IP shock impinges the magnetosphere, the *AE* index increases and the magnetospheric plasma gets hotter and denser. Their statistical studies have also suggested that IP shocks with a southward IMF pre-condition affect the magnetosphere more significantly than those with northward interplanetary magnetic field (IMF) precondition: the *AE* index usually increases from 200 to 600 nT in response to IP shocks with southward IMF precondition, which could be regarded as a signature of substorm onset, while the *AE* index enhancement is smaller (from 80 to 150 nT) for IP shocks with northward IMF. Energetic electron injections on the nightside has also been found to be related to the shock arrival. Their statistical studies reveal that substorm-like activity can be triggered by the IP shock impact. However, the physics behind the excitation of the substorm-like activity has not been explored due to the lack of comprehensive in situ observations,. Therefore, the magnetospheric response to the IP shock at the nightside sector L ~3 to 6 is crucial to understand how substorm activity is triggered by an IP shock impact.

The interaction between IP shocks and the magnetosphere is known to excite ULF wave activity [*Zong et al.*, 2009; *Zhang et al.*, 2010; *Sarris et al.*, 2010]. In the dayside magnetosphere, the ULF waves triggered by IP shocks or solar wind dynamic pressure pulses have often been observed [*Eriksson et al.*, 2006; *Zong et al.*, 2009; *Tan et al.*, 2011].

In the magnetotail, however, the excitation of ULF waves as a response to the IP shock impact is much less studied. *Tian et al.* [2012] and *Shi et al.* [2013] have reported that ULF waves can be excited in the tail plasma sheet in response to IP shock passage. Although it has been suggested that those observed ULF waves can be generated by the field line resonances in the nightside magnetosphere, the generating mechanism of IP shock-triggered ULF waves is still far from conclusive [*Tian et al.*, 2012; *Shi et al.*, 2013].

ULF waves can interact with energetic particles [*Southwood and Kivelson*, 1981, 1982; *Takahashi et al.*, 1990; *Zong et al.*, 2007]. Both electrons and ions can be accelerated by poloidal ULF waves [*Zong et al.*, 2009, 2012; *Yang et al.*, 2010]. With the recently launched Van Allen Probes mission, as *Claudepierre et al.* [2013] and *Mann et al.* [2013] pointed out, the unrivaled energy resolution could provide an excellent opportunity to study particle drift echoes and flux modulation by ULF waves, which was rather limited before due to the phase mixing effect in measurements with broader energy channels.

In this manuscript, we have presented a case study on 13 April 2013 by using Van Allen Probes observations. Our observations show that when the IP shock arrives, the response of the plasma and energetic particle activities at the nightside sector L ~3 to 6 are significantly different from both at dayside [e.g., *Zong et al.*, 2009] and in the distant tail plasma sheet [e.g., *Shi et al.*, 2013]. The magnetospheric response to the IP shock at the nightside sector L ~3 to 6 is much more complicated than previously expected. A magnetotail dipolarization is triggered initially when the IP shock impacts, followed by ULF wave (approximately 14–15 min later). The energetic electrons injection was triggered by the IP shock and the injected electrons are modulated by the ULF waves with drift resonance.

2. Data Sets

Data from the Magnetic Electron Ion Spectrometer (MagEIS) [*Blake et al.*, 2013] have been used in this study. MagEIS on each spacecraft consists of one low-energy electron detector, two medium-energy detectors, and one high-energy detector, measuring electrons from ~30 keV to 4 MeV. The operating principle of the MagEIS can be summarized as different silicon sensors recording particles of different energies and hence of different gyroradii, in a uniform magnetic field. The unprecedented resolution (25 channels) and accuracy (able to separate signal from background completely) of MagEIS measurements provide unique opportunity to study flux modulation by ULF waves. High-resolution magnetic field measurements are from a Flux Gate Magnetometer on the Electric and Magnetic Field Instrument Suite and Integrated Science (EMFISIS) [*Kletzing et al.*, 2012]. Electric field measurements are from the Electric Field and Waves Suite (EFW) [*Wygant et al.*, 2014].

3. Observations

Figures 1a–1c show the solar wind parameters recorded by Wind. A steep increase in the solar wind speed (Figure 1a) and proton density (Figure 1b) indicates an IP shock wave observed by Wind (http://umtof.umd.edu/pm/FIGS.HTML). The IMF B_z was weakly northward before the shock arrival. The shock normal was calculated to be in the GSE (−0.81, 0.17, and 0.56) direction with a compression ratio of around 3. Notice that the Wind data are shifted by 48 min, which is estimated with the downstream solar wind speed and the distance between L1 point and the subsolar point. Its geomagnetic responses are presented in Figures 1d and 1e. A positive pulse of 10 nT in the B_H component was observed at 22:54 UT at the SHU station (55.35 °N, LT = 12.2 at 22:54 UT). After shifting the IP shock profile, the noonside positive B_H pulse lags the IP shock by less than 2 min, implying that the pulse might be a magnetosonic wave generated when the shock impinged the magnetopause and propagates earthward. The *AE* index increased by 150 nT within 15 min after the shock arrival, which is consistent with the statistical study by *Yue et al.* [2010].

The nightside magnetospheric plasma responses are shown in Figure 2. Van Allen Probes were in the nightside, Northern Hemisphere near the equatorial plane. Located at their apogee with an L shell of 4.8–5.7, they provide an excellent opportunity to study the midnight magnetic field and particle response to the shock. As shown in Figure 2c, the angle between the nightside magnetic field and GSM X-Y plane ($\arctan\frac{B_z}{B_x}$) suddenly increased by 2° ~ 3° after the shock arrival and gradually recovered about 14 min after the shock passage, which indicates that the nightside magnetic field was compressed to a more dipole-like configuration by the shock passage.

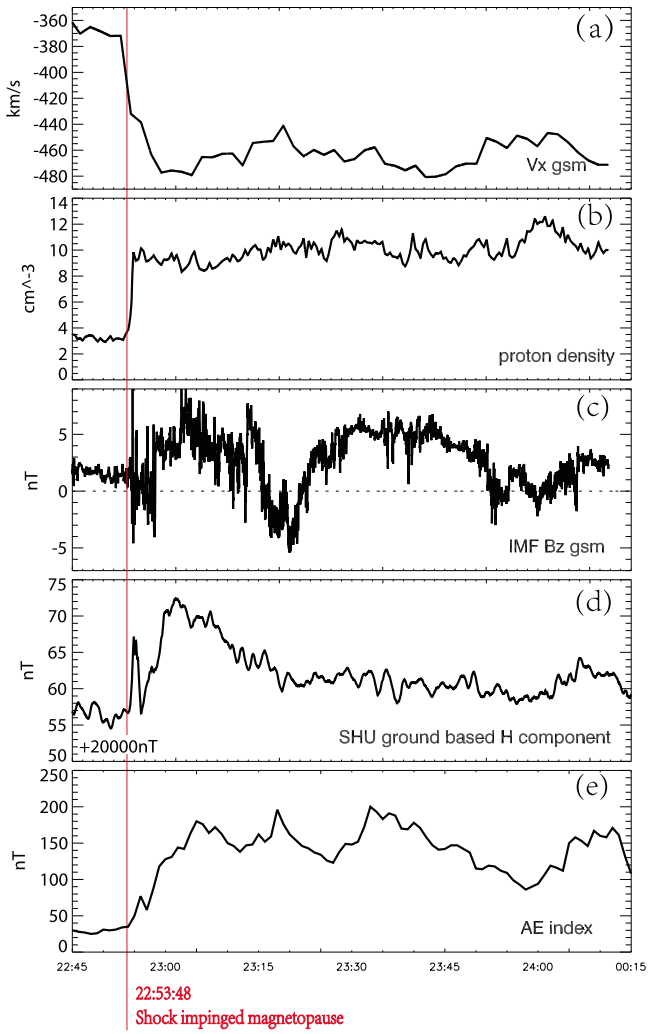

Figure 1. Overview of the solar wind parameters observed by Wind and the corresponding response. (a) *X* component of the solar wind velocity in GSM coordinate system. (b) Proton density. (c) Interplanetary B_{zGSM}. (d) B_H measured at Alaska (SHU) ground magnetometer station. (e) *AE* index. Notice that Figures 1a–1c are shifted 48 min right. The shock arrival time is marked with a vertical red line.

Immediately after the shock passage, the energetic electron flux (30–500 keV) experienced a sudden enhancement, followed by typical drift echoes (Figures 2a and 2b). The observed drift echoes imply that the electron flux enhancement was a localized injection rather than a global electron flux sudden enhancement. The absence of clear dispersion in the initial injection indicates that the Van Allen Probes were located near the source region [*Reeves et al.*, 1990; *Sarris and Li*, 2005]. Two to three cycles of flux variation followed the initial injection. The time intervals between the peaks of these cycles vary from 226 s to 301 s, indicating that these variations were not exactly sinusoidal.

To investigate the direction of energy transport, the Poynting vector is calculated with measurements from EFW-A and EMFISIS-A. Note that 10 min smoothing operation is carried out in order to show the main direction of the energy flux. As shown in Figure 2d, the energy flux was mostly tailward and equatorward during the magnetic field reconfiguration and turned earthward during the ULF wave activity, as we will present below. Plasma bulk flow velocity is calculated using $V = E \times B/|B|^2$ (see Figure 2e). The *x* component of plasma velocity in GSM coordinate was strongly negative immediately after the shock arrival and turned slightly positive 9 min later.

Periodic variations in electric and magnetic fields in ULF wave band emerged 14 min after the shock arrival (see Figure 2c), along with 150 s quasiperiodic variations of electron fluxes of good monochromaticity (Figures 2a and 2b). The electric and magnetic fields are projected to a local mean field-aligned (MFA) coordinate system [e.g., *Takahashi et al.*, 1990] in order to analyze the oscillation properties; the MFA coordinate system is determined by 15 min sliding average EMFISIS magnetic field data (Figure 3a∼c and 3e∼g). To analyze the electron flux modulation, the residual electron flux is calculated (Figures 3d and 3h). Residual flux is defined by *Claudepierre et al.* [2013] as $\frac{J-J_0}{J_0}$, where *J* is the flux observed in each MagEIS energy channel and J_0 is a 10 min, running boxcar average of *J*. The results after the coordinate transformation show strong oscillations in the radial component of the magnetic field and the azimuthal component of the electric field, while the amplitude in B_a and E_r is relatively small. This indicates that the ULF waves detected were dominated by the poloidal mode. Observations from both satellites show that a short period (60–90 s) oscillation (transient Pi2 mode) of large amplitude lasted for 3–7 cycles and was quickly damped. A steady, monochromatic long-period (around 150 s) ULF wave (Pc 4–5 band) took over and modulated the electron flux for around 1 h. As shown in Figures 3d and 3h, the fluxes of electrons with energy up to 450 keV show clear sinusoidal variations in the observed ULF wave band.

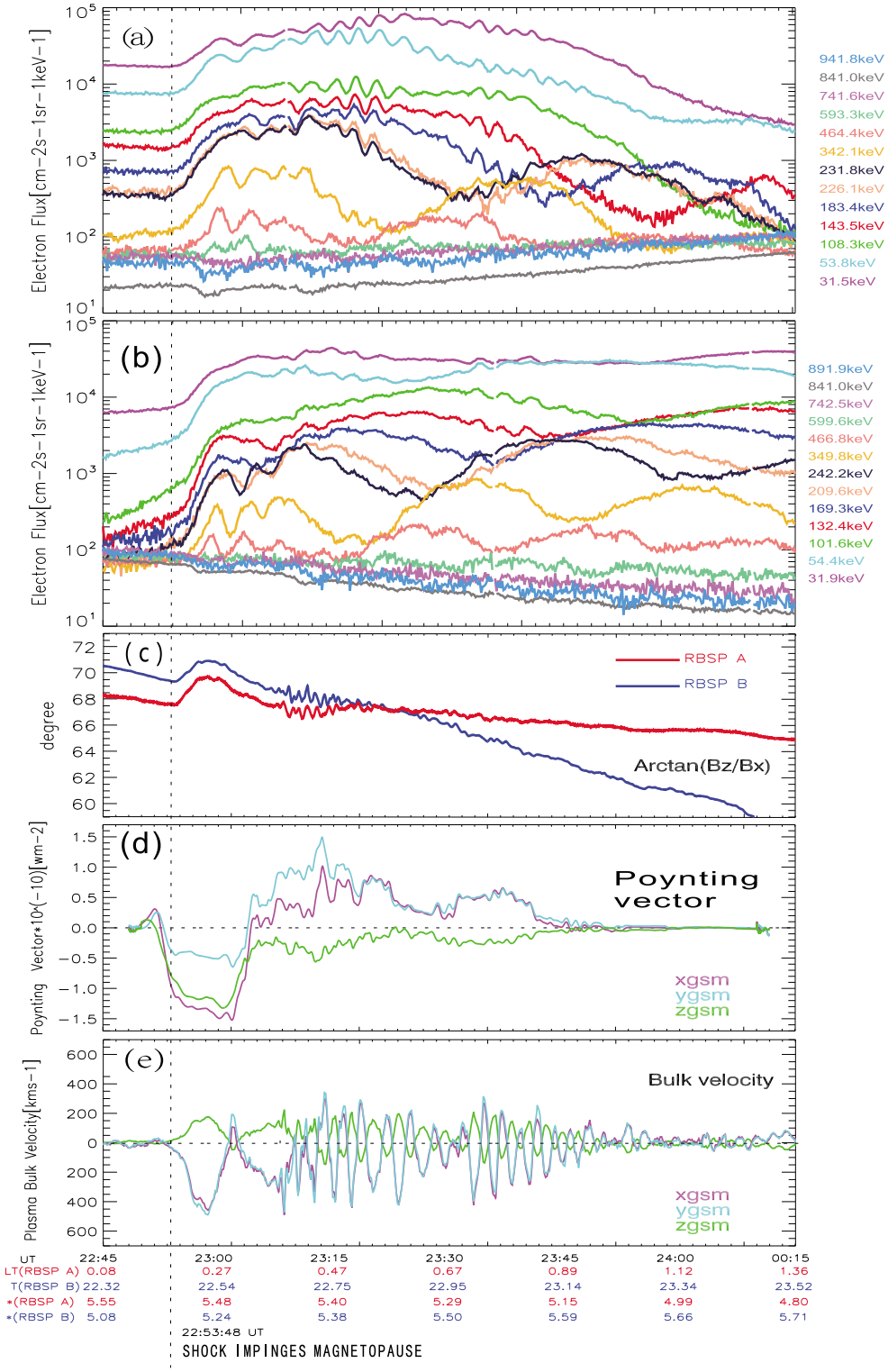

Figure 2. Observations of electron differential flux and plasma parameters by Van Allen Probes A and B. (a) Spin-averaged, differential electron flux from MagEIS-A. (b) Similar to Figure 2a but from MagEIS-B. (c) Calculated arctan $(\frac{B_{zGSM}}{B_{xGSM}})$ using magnetic field measured by EMFISIS-A and -B. (d) Smoothed Poynting vector in GSM coordinate calculated with data from probe A. (e) Plasma bulk velocity calculated from $V = \frac{E \times B}{|B|^2}$.

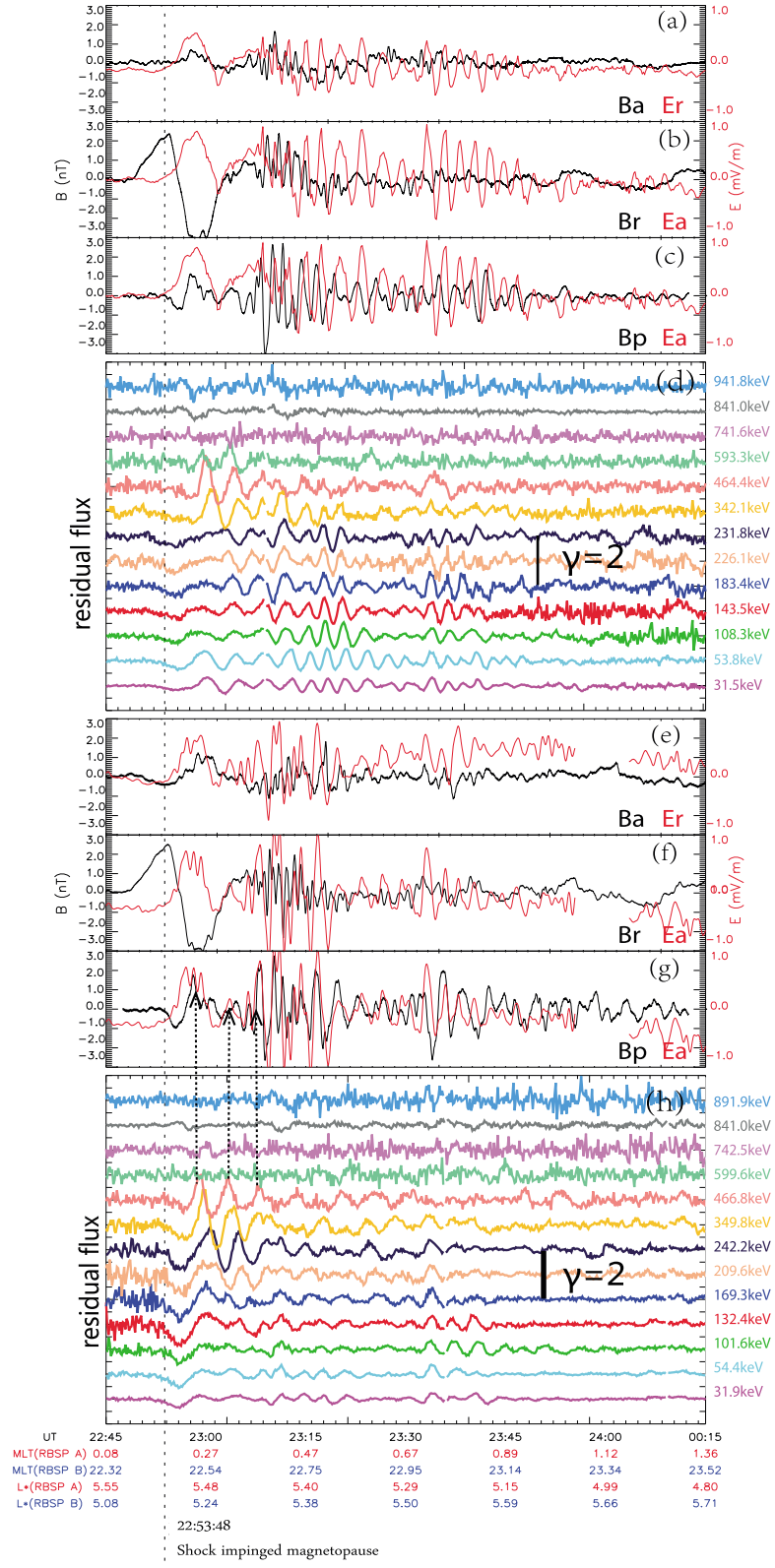

Figure 3. Electromagnetic field measured by EFW-A and EMFISIS-A in MFA coordinates. (a) The azimuthal component of the magnetic field and radial component of the electric field. (b) The radial component of magnetic field and the azimuthal component of the electric field. (c) Detrended parallel component of the magnetic field and the azimuthal component of the electric field. (d) Residual electron flux $\frac{J-J_0}{J_0}$. (e–h) Similar to Figures 3a–3d but for Van Allen Probe B. The dashed arrows mark the electric field possibly responsible for the multiple injections.

Table 1. Determining Harmonic Mode Through Phase Analysis

$\theta(E_a) - \theta(B_r)$	Northern Hemisphere	Southern Hemisphere
Odd mode	−90°	+90°
Even mode	+90°	−90°

4. Interpretation and Discussion

In the previous section, a shock-induced nightside ULF wave case is reported. Note that the time profile of both field and particles in this case differs distinctively from either dayside shock-induced ULF waves [e.g., *Zong et al.*, 2009] or ULF waves excited in plasma sheet [e.g., *Shi et al.*, 2013]. Although energetic particle injections, nightside ULF waves, and charged particle modulation by these waves have been separately reported before, our case study reveals that they are all triggered by an IP shock in this event, in a specific sequence of events. In this section, we present a detailed study on the properties of the ULF waves and their modulation of injected electrons. Two competitive mechanisms on ULF wave excitation are also discussed.

4.1. ULF Waves and Multiple Injections Observed in the Nightside Magnetosphere

Transverse Alfvén wave can be divided into propagating wave and standing wave. For standing waves, the electric field and magnetic fields are 90° out of phase, while propagating waves are in phase or 180° out of phase [e.g., *Singer et al.*, 1982]. The steady ULF waves with a period of 150 s observed by the Van Allen Probes shows a clear 90° phase difference between E_a and B_r, indicating a standing wave mode. This suggests that the transverse wave detected satisfied the field line resonance (FLR) condition. For each satellite, E_a and E_r detected are mostly in phase, thus quasi-linearly polarized.

Odd and even harmonic mode ULF waves act differently in the magnetosphere, which can help us determine the harmonic mode. *Singer et al.* [1982] pointed out that odd and even harmonic waves show opposite phase differences between the magnetic field and electric field. *Zong et al.* [2011] suggested that only fundamental wave modulates energetic electrons efficiently considering that their bounce frequency is incomparably larger than their drift frequency, and the effect of acceleration approximately counterbalances the effect of deceleration in even modes. Both clear 90° phase difference between E_a and B_r and significant energetic electron flux modulation (tens to hundreds keV) in this study are in favor of fundamental harmonic poloidal Pc 4–5 wave (see Table 1) observed in the Northern Hemisphere.

As we have mentioned above, 2–3 cycles of flux variation following the initial injection of 30–500 keV electrons were observed by both spacecraft. Note that these seemingly quasiperiodic variations are distinctively different from the following steady flux modulation by ULF wave, for the time interval between peaks of these variations was between 226 s and 301 s, while the local eigenfrequency of fundamental harmonic FLR is approximately 150 s. We suggest that the time profile recorded by MagEIS can possibly be interpreted as multiple injections, which have been reported in simulation work before [*Ebihara and Tanaka*, 2013]. *Ebihara and Tanaka* [2013] suggested that the multiple injections are driven by electric field induced by pressure imbalance during the injection process. We have marked the electric field signals that might be responsible for the multiple injections in Figure 3. Significant electric field signals responsible for the second and third injections were not observed by Van Allen Probes A. MagEIS observations show that the second and third injections appeared in the 200–500 keV record of Van Allen Probes A (0.27 MLT) about 30 s later than the spacecraft B (22.54 MLT). Hence, the following injections observed by Van Allen Probes A can be interpreted as electrons drifting from westward accelerating area.

4.2. Poloidal ULF Wave Number

With Van Allen Probes close to each other, we can extract the azimuthal wave mode number from the electromagnetic field measurements [*Takahashi et al.*, 1985].

The azimuthal wave number is given by

$$m = \frac{\Delta\theta}{\Delta\phi}$$

where m is the azimuthal wave number, $\Delta\theta$ stands for the phase angle difference of the ULF waves measured by two Van Allen Probes, and $\Delta\phi$ is the azimuthal angle separation of the two probes.

Cross-wavelet analysis [*Grinsted et al.*, 2004] is performed to calculate the phase angle difference of the electric field. As shown in Figure 4, for the time interval when the coherence larger than 0.8, the phase difference of E_a is possibly $0 \pm 10°$, $360 \pm 10°$, $720 \pm 10°$, $1080 \pm 10°$, and so on. Given that the magnetic local time (MLT)

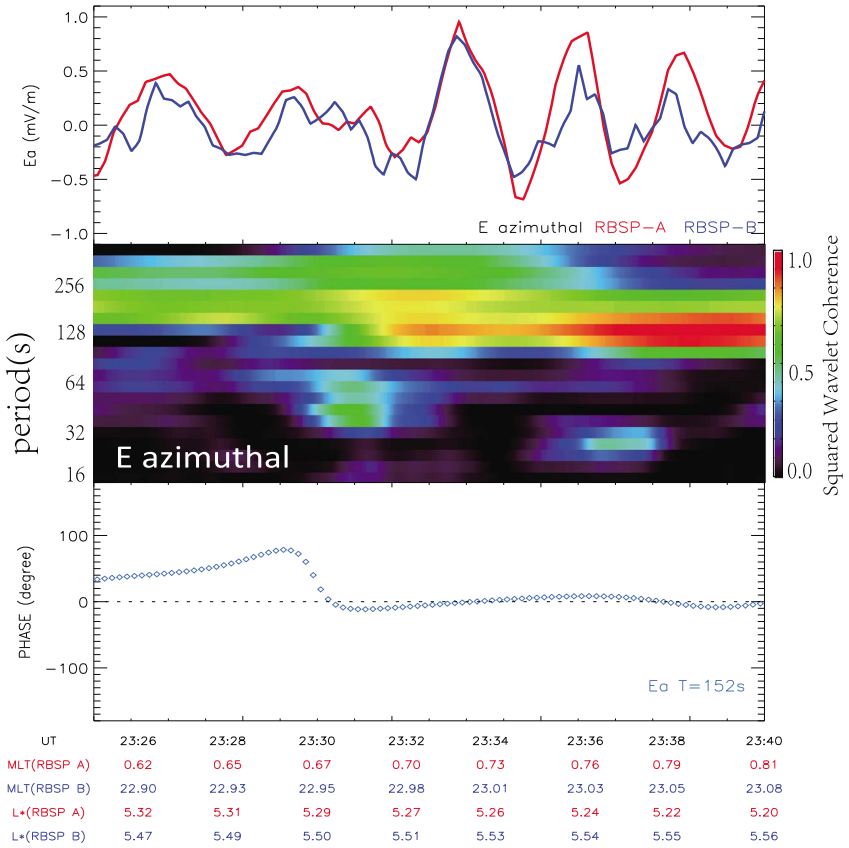

Figure 4. (top to bottom) E_a observed by Van Allen Probes A and B. The squared wavelet coherence between the E_a by Probes A and B. Phase difference between electric field measured by Van Allen Probes A and B, obtained from cross-wavelet analysis.

difference between Van Allen Probes A and B is from 1.72 to 1.73 h, m can be ~0, 14, 28, 42, or larger (more precisely, ±0.39, 13.48 to 14.34, 27.36 to 28.29, or 41.23 to 42.25 or larger).

This ambiguity may be eliminated by examining the characters of resonant particles during the wave-particle interaction [*Zong et al.*, 2007].

The theory on interactions between ULF poloidal waves and energetic particles has been developed by *Southwood and Kivelson* [1981, 1982]. The resonance occurs when the following condition is satisfied:

$$\omega - m\omega_d = N\omega_b \tag{1}$$

where ω, ω_d, and ω_b are wave angular frequency, angular drift frequency, and angular bounce frequency, respectively, m represents the azimuthal wave mode number, and N is an integer. For electrons, the bounce frequency is orders of magnitude higher than the drift frequency. Thus, $N = 0$ is the only possible resonance condition for energetic electrons [e.g., *Zong et al.*, 2007; *Ozeke and Mann*, 2008], so the resonance condition turns to be

$$\omega = m\omega_d \tag{2}$$

According to the theory developed by *Southwood and Kivelson* [1981], resonant particle flux oscillates strictly in phase or antiphase with E_a, while nonresonant particle flux oscillates 90° out of phase with E_a, which can be used to determine the resonant energy [e.g., *Zong et al.*, 2007; *Dai et al.*, 2013]. As we can see from Figure 4, particles with the energy of 183 keV and 226 keV are most closely oscillating in phase with the azimuthal component of the electric field (see Figure 5). The in-phase oscillations suggest that drift resonance was excited in these channels.

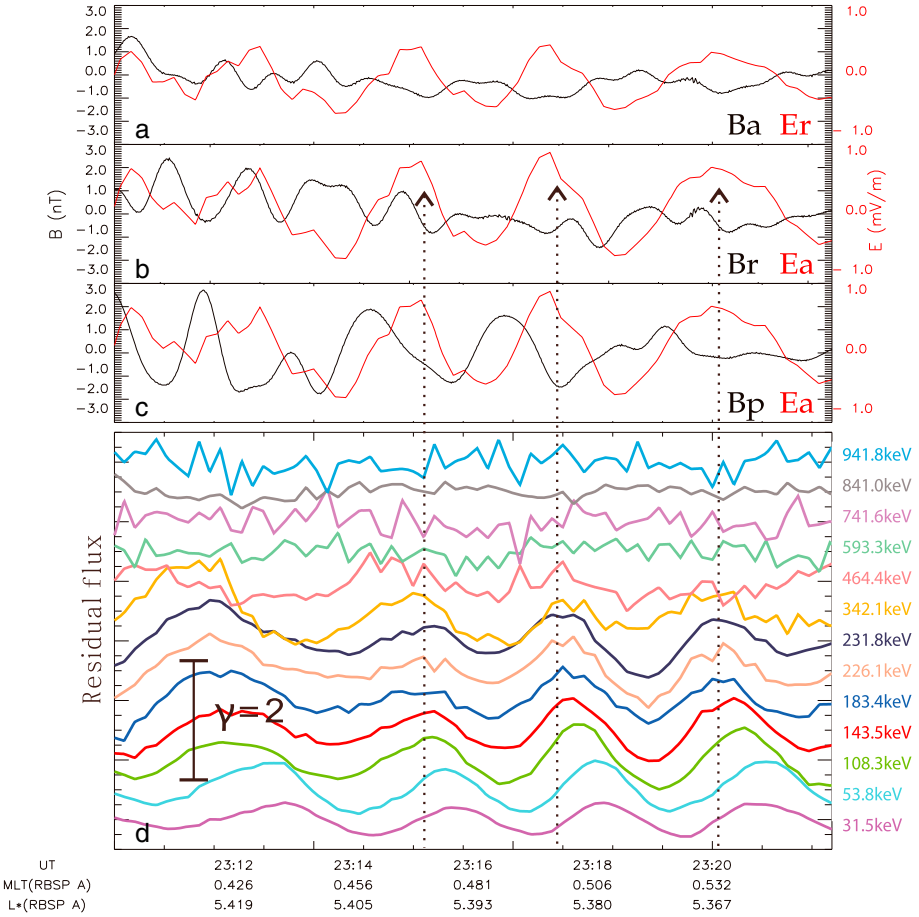

Figure 5. (a–c) Similar to Figures 3a–3c but from 23:10 UT to 23:22 UT. (d) Residual flux measured by Van Allen Probes A. Notice that for electrons with resonant energy (150 keV to 230 keV), the electron flux is mostly in phase with E_a, while ±90° out of phase for higher or lower energies.

The obtained energy channels of strong resonant effect (183 keV and 226 keV) are also confirmed by peak-to-valley ration estimation of the particle flux oscillations. The relevant flux peak-to-valley ratio (γ) at the resonant energy should be larger than adjacent energies [*Yang et al.*, 2010], assuming that the spatial gradient of electrons does not vary intensively among the energy channels. As shown in Figure 2, the electron fluxes in the present case are highly dynamic by mixing the flux modulation due to wave-particle interactions and drift echoes due to substorm-like injection. Thus, the peak-to-valley ratio of each energy channel cannot be obtained simply because of the existence of electron drift echoes.

In order to estimate the peak-to-valley ratio more precisely, first, we select the time period from 23:30 to 23:45 UT, during which the signature of the particle flux modulation is very clear and the substorm-like initial particle injection signal is excluded. Secondly, only the peak-to-valley ratio $\gamma > 1.2$ is selected for the wave modulated flux oscillation for each energy channel [*Yang et al.*, 2010].

The obtained the peak-to-valley ratio for each energy channel is given in Figure 6. The ratios may contain either overestimated or underestimated ratios due to the preexisting trend caused by drift echoes. The average peak-to-valley ratios for each energy channel are plotted in a red line in Figure 6.

As shown in Figure 6, we have obtained a typical resonance curve. It can be clearly seen that strong resonant value appears at the energy channels of 183 and 226 keV, consistent with the channels we have through phase comparing. Further, the resonant energy width can be obtained from Figure 6 by defining the resonance width at $\frac{\max+\min}{2}$ rather than using the traditional full width at half maximum since the flux variation due to nonresonance effect will also contribute to the peak-to-valley ratio. With the definition above, the resonant energy is measured to be from 150 keV to 230 keV. The resonant bandwidth is

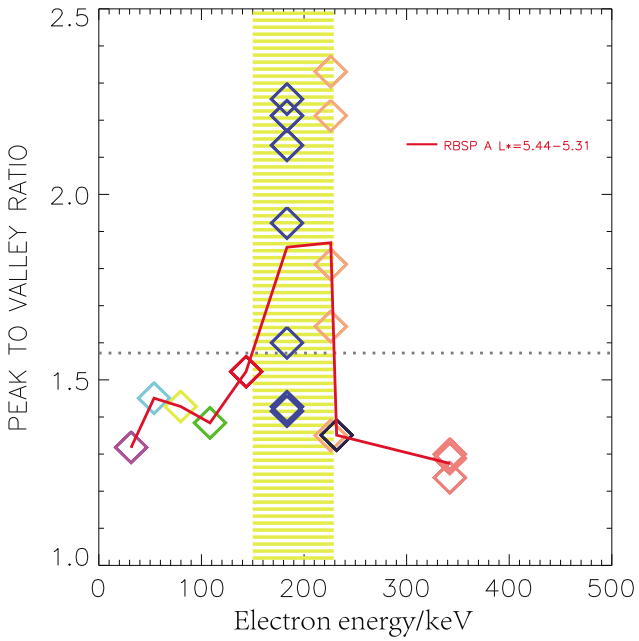

Figure 6. The peak-to-valley ratio of the electron flux from 23:30 UT to 23:45 UT measured by MagEIS-A. Diamonds represent the peak-to-valley ratio of each energy channel. The red line represents the average peak-to-valley ratios for each channel, dashed line for $\frac{\max+\min}{2}$ of the red line and yellow background for full width at $\frac{\max+\min}{2}$ (max = 1.87 and min = 1.27).

estimated to be around 80 keV, which can be explained as a spread in the resonant energy, as suggested by *Takahashi et al.* [1990]. The estimated resonant energy bandwidth can be confirmed by the drift resonance condition. The ratio between the bandwidth and the resonant energy ($\frac{\Delta E}{E}$) is around 0.4. Spectrum analysis has shown that the power of the E_a component of the ULF wave peaks at 6.6 mHz with a bandwidth of 2.8 mHz. Thus, $\frac{\Delta\omega}{\omega}$ of the ULF wave is also around 0.4. Considering the drift resonance condition (equation (1)), the spread of the resonant energy can mainly be interpreted as the finite bandwidth of the ULF wave.

The resonant energy obtained above can also be utilized to estimate the azimuthal wave number. We have figured out that obtained electron resonant energy is around 200 keV at L ~5.3 and the observed poloidal wave period is around 150 s. With the pitch angle data measured by MagEIS, the average sin(PA) for electrons in the resonant energy from 23:30 UT to 23:40 UT is estimated to be around 0.8. Thus, the azimuthal wave number estimated according to the drift resonance condition is 16–19, which is fairly consistent with the wave number (m ~14) derived from multiple spacecraft observations. We note that both methods for m value estimating discussed above involve some ambiguity. Although multispacecraft ULF wave phase comparing is more direct and of more accuracy, there is ambiguity of $2k\pi$ when the satellites are located with large angular separation. Such ambiguity does not affect the resonant condition, however, the calculated m value in this way is of lower accuracy for the finite bandwidth of both the energy channel and the ULF wave frequency. Combining the two methods, we have figured out the azimuthal wave number of the ULF wave excited to be ~14.

4.3. Excitation of the ULF Waves in the Magnetotail

How are the observed ULF waves in the magnetotail excited? There are two possible mechanisms: flow-driven FLR and injected particle driven drift-bounce resonance instability.

Sibeck [1990] proposed a model for the shock/magnetosphere interaction based on the force balance between the transient solar wind and the magnetopause/magnetosphere. In his model, a single or double vortex around the magnetopause will be generated when an IP shock with a high dynamic pressure is impinged on the magnetopause. As a result, inside the magnetosphere, a fast-mode compressional wave can be excited. The fast-mode wave usually propagates tailward faster than the IP shock propagating in the solar wind [*Sibeck*, 1990]. Further, this will cause the magnetopause to bulge outward ahead of the IP shock and subsequently will cause an inward compression of the magnetopause after the IP shock. These outward and inward bulges in turn generate vortex-like structures inside the magnetosphere [*Sibeck*, 1990].

As shown in Figures 2d and 2e, the electromagnetic Poynting flux and plasma flow obtained from the frozen-in condition $E = -V \times B$ are exhibiting a bipolar signature with initially negative (positive) that turns into positive (negative) immediately after the IP shock passage. These indicate that a vortex has been observed, also, Such a IP shock induced vortex-like flow has been also observed by *Huttunen et al.* [2005], *Keika et al.* [2008], *Tian et al.* [2012], and *Shi et al.* [2013] in the tail plasma sheet.

The generated vortex-like plasma flow structure will further excite Alfvén waves at certain frequencies depending on the azimuthal phase velocity of the plasma flow structure. The fast-mode compressional wave

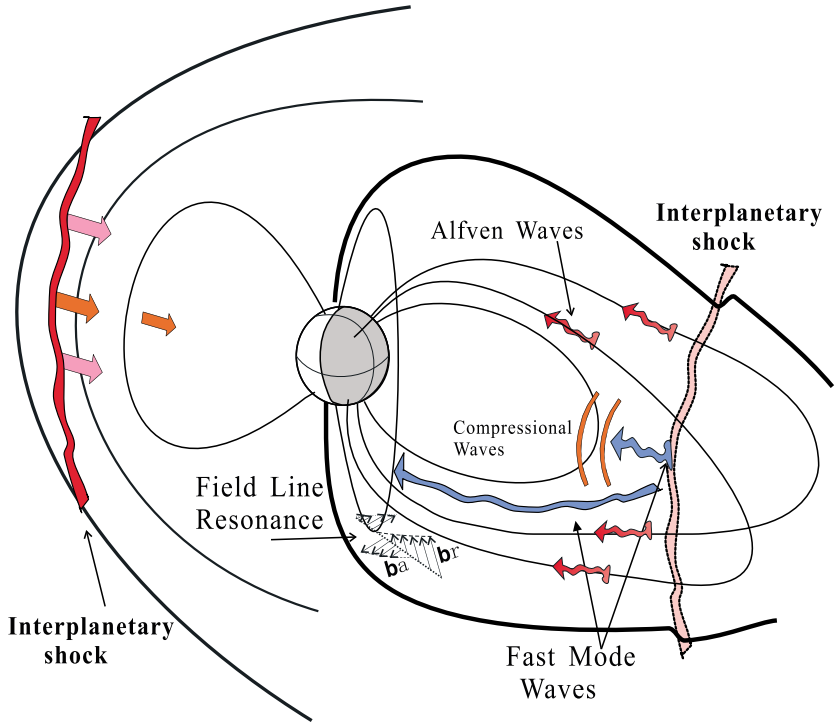

Figure 7. A schematic sketch showing the possible dynamic process in this case. Pressure enhancement associated with the interplanetary shock drives reconfiguration in the nightside magnetosphere. At L ~5 , it breaks the dynamic balance and causes particle injection. At deeper tail, vortex-like plasma flow is generated. The flow vortex acts as a broadband spectrum motion that drives compressional waves. The earthward-propagating fast-mode compressional waves drive field line resonance (FLR) at a certain L shell. The excited poloidal standing Alfvén waves in Pc 4–5 band interact with energetic particles through drift-bounce resonance.

will act as an intermediary that transport the magnetopause motion's energy to a location of Alfvén resonance [*Wright and Rickard*, 1995]. As the fast-mode wave propagates toward the magnetosphere, the field line resonance can be excited; this scenario is shown in Figure 7. Further, the excited wave would interact with the drifting energetic electrons through drift resonance, which is similar to the IP shock excited dayside ULF wave scenario developed by *Zong et al.* [2009, 2012].

Another possible scenario is that poloidal ULF waves can be excited theoretically through bounce-drift resonance [*Southwood and Kivelson*, 1981]. Further, *Ozeke and Mann* [2008] suggested that energetic ring current ions can excite poloidal ULF wave of moderate m number in the second harmonic. Also, fundamental poloidal mode was found to be possibly related to east drifting injected electrons [*James et al.*, 2013]. As shown in Figure 2, the observed dispersionlessly injected energetic electrons could excite the poloidal mode ULF waves (first harmonic) through the drift-bounce resonance. However, it is difficult to use this scenario to explain that (1) both poloidal and toroidal mode ULF waves are excited simultaneously and are dampened at the same rate; (2) the observed ULF waves have a rather long time delay (~14 min) with respect to the injected energetic electron.

Therefore, the first scenario is more favorable to explain the observations in the present paper while the second scenario could not be ruled out completely.

5. Summary

As shown in the above sections, an IP shock-induced substorm-like event on 13 April 2013 has been observed in the nightside magnetosphere by both Van Allan Probes. Substorm-like electron injections with energy of 30–500 keV have been observed in regions from L ~5.2 to 5.5 immediately after the IP shock impinge on the magnetosphere. The electron flux oscillated strongly on the ULF wave scale. By examining both the electric field and magnetic field data, it is found that both toroidal and poloidal mode ULF waves with a period of 150 s emerged following the magnetotail magnetic field reconfiguration after the IP shock

arrival. The poloidal mode ULF is more intense than the toroidal one. The dominant fundamental poloidal waves lasted for more than 1 h.

Further, a 90° phase shift between the poloidal mode B_r and E_a along with the energetic electron flux modulation indicate that the dominant poloidal standing wave observed at the Northern Hemisphere are fundamental harmonic. Direct evidence of drift resonance between the injected electrons and the excited poloidal ULF wave has been obtained. The resonant energy is estimated to be between 150 keV and 230 keV. The resonant energy width is estimated by measuring the full width at $\frac{\max+\min}{2}$ in peak-to-valley ratio. Both the evidence from multiple spacecraft field measurements and wave-particle resonance are engaged to derive the azimuthal wave number of the observed ULF wave, and the azimuthal wave number is estimated to be ~14.

Acknowledgments

This work was supported by Major Project of Chinese National Programs for Fundamental Research and Development (2012CB825603) and National Natural Science Foundation of China (40831061, 41074117, and 41050110440). We acknowledge Space Physics Data Facility, Goddard Space Flight Center (http://cdaweb.gsfc.nasa.gov/) for providing all data in this article. Thanks to Jane Su and Jie Ren for useful discussion.

Michael Liehmon thanks two anonymous reviewers for their assistance in evaluating this paper.

References

Blake, J., et al. (2013), The Magnetic Electron Ion Spectrometer (MagEIS) instruments aboard the Radiation Belt Storm Probes (RBSP) spacecraft, *Space Sci. Rev.*, 1–39.

Claudepierre, S. G., I. R. Mann, K. Takahashi, J. F. Fennell, M. K. Hudson, and J. B. Blake (2013), Van Allen probes observation of localized drift resonance between poloidal mode ultra-low frequency waves and 60 keV electrons, *Geophys. Res. Lett.*, *40*, 4491–4497, doi:10.1002/grl.50901.

Dai, L., et al. (2013), Excitation of poloidal standing Alfvén waves through drift resonance wave-particle interaction, *Geophys. Res. Lett.*, *40*, 4127–4132, doi:10.1002/grl.50800.

Ebihara, Y., and T. Tanaka (2013), Fundamental properties of substorm time energetic electrons in the inner magnetosphere, *J. Geophys. Res. Space Physics*, *118*, 1589–1603, doi:10.1002/jgra.50115.

Eriksson, P. T. I., L. G. Blomberg, S. Schaefer, and K. H. Glassmeier (2006), On the excitation of ULF waves by solar wind pressure enhancements, *Ann. Geophys.*, *24*, 3161–3172.

Gosling, J., D. McComas, J. Phillips, and S. Bame (1991), Geomagnetic activity associated with earth passage of interplanetary shock disturbances and coronal mass ejections, *J. Geophys. Res.*, *96*, 7831–7839.

Gosling, J. T. (1993), The solar flare myth, *J. Geophys. Res.*, *98*(A11), 18,937–18,949, doi:10.1029/93JA01896.

Grinsted, A., J. C. Moore, and S. Jevrejeva (2004), Application of the cross wavelet transform and wavelet coherence to geophysical time series, *Nonlinear Process. Geophys.*, *11*, 561–566.

Huttunen, K. E. J., J. Slavin, M. Collier, H. E. J. Koskinen, A. Szabo, E. Tanskanen, A. Balogh, E. Lucek, and H. Rème (2005), Cluster observations of sudden impulses in the magnetotail caused by interplanetary shocks and pressure increases, *Ann. Geophys.*, *23*(2), 609–624, doi:10.5194/angeo-23-609-2005.

James, M., T. Yeoman, P. Mager, and D. Y. Klimushkin (2013), The spatio-temporal characteristics of ULF waves driven by substorm injected particles, *J. Geophys. Res. Space Physics*, *118*, 1737–1749, doi:10.1002/jgra.50131.

Keika, K., et al. (2008), Response of the inner magnetosphere and the plasma sheet to a sudden impulse, *J. Geophys. Res.*, *113*, A07S35, doi:10.1029/2007JA012763.

Kletzing, C., et al. (2012), The Electric and Magnetic Field Instrument Suite and Integrated Science (EMFISIS) on RBSP, *Space Sci. Rev.*, *179*, 127–181.

Mann, I. R., et al. (2013), Discovery of the action of a geophysical synchrotron in the Earth's Van Allen radiation belts, *Nat. Commun.*, *4*, 2795, doi:10.1038/ncomms3795.

Nishida, A., and K. Maezawa (1971), Two basic modes of interaction between the solar wind and the magnetosphere, *J. Geophys. Res.*, *76*, 2254–2264.

Ozeke, L. G., and I. R. Mann (2008), Energization of radiation belt electrons by ring current ion driven ULF waves, *J. Geophys. Res.*, *113*, A02201, doi:10.1029/2007JA012468.

Reeves, G. D., T. A. Fritz, T. E. Cayton, and R. D. Belian (1990), Multi-satellite measurements of substorm injection region, *Geophys. Res. Lett.*, *17*, 2015–2018.

Sarris, T., and X. Li (2005), Evolution of the dispersionless injection boundary associated with substorms, *Ann. Geophys.*, *23*, 877–884.

Sarris, T., W. Liu, X. Li, K. Kabin, E. Talaat, R. Rankin, V. Angelopoulos, J. Bonnell, and K.-H. Glassmeier (2010), THEMIS observations of the spatial extent and pressure-pulse excitation of field line resonances, *Geophys. Res. Lett.*, *37*, L15104, doi:10.1029/2010GL044125.

Shi, Q. Q., et al. (2013), Themis observations of ULF wave excitation in the nightside plasma sheet during sudden impulse events, *J. Geophys. Res. Space Physics*, *118*, 284–298, doi:10.1029/2012JA017984.

Sibeck, D. G. (1990), Evidence for flux rope in the Earth's magnetotail, in *Physics of Magnetic Flux Ropes, Geophys. Monogr. Ser.*, vol. 58, edited by C. T. Russell, E. R. Priest, and L. C. Lee, pp. 637–646, AGU, Washington, D. C.

Singer, H. J., W. J. Hughes, and C. T. Russell (1982), Standing hydromagnetic waves observed by ISEE 1 and 2: Radial extent and harmonic, *J. Geophys. Res.*, *87*, 3519–3529.

Southwood, D. J., and M. G. Kivelson (1981), Charged particle behavior in low-frequency geomagnetic pulsations. I. Transverse waves, *J. Geophys. Res.*, *86*, 5643–5655.

Southwood, D. J., and M. G. Kivelson (1982), Charged particle behavior in low-frequency geomagnetic pulsations. II. Graphical approach, *J. Geophys. Res.*, *87*, 1707–1710.

Takahashi, K., P. R. Higbie, and D. N. Baker (1985), Azimuthal propagation and frequency characteristic of compressional Pc 5 waves observed at geostationary orbit, *J. Geophys. Res.*, *90*, 1473–1485.

Takahashi, K., R. W. McEntire, A. T. Y. Lui, and T. A. Potemra (1990), Ion flux oscillations associated with a radially polarized transverse Pc 5 magnetic pulsation, *J. Geophys. Res.*, *95*, 3717–3731.

Tan, L. C., X. Shao, A. S. Sharma, and S. F. Fung (2011), Relativistic electron acceleration by compressional mode ULF waves: Evidence from correlated Cluster, Los Alamos National Laboratory spacecraft, and ground based magnetometer measurements, *Geophys. Res. Lett.*, *116*, A07226, doi:10.1029/2010JA016226.

Tian, A., et al. (2012), Dynamics of long-period ULF waves in the plasma sheet: Coordinated space and ground observations, *J. Geophys. Res.*, *117*, A03211, doi:10.1029/2011JA016551.

Wright, A. N., and G. J. Rickard (1995), A numerical study of resonant absorption in a magnetohydrodynamic cavity driven by a broadband spectrum, *Astrophys. J.*, *444*, 458–470.

Wygant, J., et al. (2014), The electric field and waves instruments on the radiation belt storm probes mission, *Space Sci. Rev.*, *179*, 183–220, doi:10.1007/s11214-013-0013-7.

Yang, B., Q. Zong, Y. F. Wang, S. Y. Fu, P. Song, H. S. Fu, A. Korth, T. Tian, and H. Reme (2010), Cluster observations of simultaneous resonant interactions of ULF waves with energetic electrons and thermal ion species in the inner magnetosphere, *J. Geophys. Res.*, *115*, A02214, doi:10.1029/2009JA014542.

Yue, C., Q. G. Zong, and Y. F. Wang (2009), Response of the magnetic field and plasmas at the geosynchronous orbit to interplanetary shock, *Chin. Sci. Bull.*, *54*, 4241–4252.

Yue, C., Q. G. Zong, Y. Wang, I. I. Vogiatzis, Z. Pu, S. Fu, and Q. Shi (2011), Inner magnetosphere plasma characteristics in response to interplanetary shock impacts, *J. Geophys. Res.*, *116*, A11206, doi:10.1029/2011JA016736.

Yue, C., Q. G. Zong, H. Zhang, Y. F. Wang, C. J. Yuan, Z. Y. Pu, S. Y. Fu, A. T. Y. Lui, B. Yang, and C. R. Wang (2010), Geomagnetic activities triggered by interplanetary shocks, *J. Geophys. Res.*, *115*, A00I05, doi:10.1029/2010JA015356.

Zhang, X. Y., Q.-G. Zong, Y. F. Wang, H. Zhang, L. Xie, S. Y. Fu, C. J. Yuan, C. Yue, B. Yang, and Z. Y. Pu (2010), ULF waves excited by negative/positive solar wind dynamic pressure impulses at geosynchronous orbit, *J. Geophys. Res.*, *115*, A10221, doi:10.1029/2009JA015016.

Zong, Q.-G., et al. (2007), Ultralow frequency modulation of energetic particles in the dayside magnetosphere, *Geophys. Res. Lett.*, *34*, L12105, doi:10.1029/2007GL029915.

Zong, Q.-G., X.-Z. Zhou, Y. F. Wang, X. Li, P. Song, D. N. Baker, T. A. Fritz, P. W. Daly, M. Dunlop, and A. Pedersen (2009), Energetic electrons response to ULF waves induced by interplanetary shocks in the outer radiation belt, *J. Geophys. Res.*, *114*, A10204, doi:10.1029/2009JA014393.

Zong, Q.-G., Y. F. Wang, and C. J. Yuan (2011), Fast acceleration of "killer" electrons and energetic ions by interplanetary shock stimulated ULF waves in the inner magnetosphere, *Chin. Sci. Bull.*, *56*, 1188–1201, doi:10.1007/s11,434–010–4308–8.

Zong, Q.-G., Y. Wang, H. Zhang, S. Fu, C. Wang, C. Yuan, and I. Vogiatzis (2012), Fast acceleration of inner magnetospheric hydrogen and oxygen ions by shock induced ULF waves, *J. Geophys. Res.*, *117*, A11206, doi:10.1029/2012JA018024.